Validation and Calibration of the Large Area Telescope Effective Area Using Two Years of Flight Data

E. Charles (SLAC), P. Bruel (Ecole Polytechnique,CNRS/IN2P3), R. Buehler (SLAC/ KIPAC), T. Johnson (U. Maryland & NASA GSFC), R. Rando (INFN Padova)
on behalf of the Fermi Large Area Telescope Collaboration

After two years of observations the LAT flight data set itself is by far the best source of calibration data available. The LAT team has used a variety of techniques and calibration sources to derive in-flight calibrations of the LAT Effective Area. In particular, we have used phase-gated selections of photons from bright pulsars, as well as other bright sources such as Active Galactic Nuclei (AGN) and the Earth Limb to show that the efficiency of our photons selections on flight data closely matches the efficiencies we derived from detailed Monte Carlo simulations of photon interactions with the LAT. In the few cases where we found significant disagreement between simulations and flight data we quantified the discrepancies and used them to derive corrected Effective Area tables.

1) Effective Area (A_{eff}) from simulations

As described in (1) our effective area calibrations are based on detailed Monte Carlo (MC) simulations of photons with a model of the Fermi-LAT.
We parameterize the A_{eff} as a function of energy and the cosine of angle of the incident photon with respect to the LAT boresight (cos(θ)). Fig. 1 shows an example A_{eff} table.

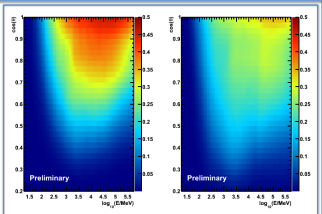

Fig. 1) A_{eff} of the LAT for the P7_SOURCE event selection for front (left) and back (right) converting events. The color scale is in m². Note the large variation with both energy and incident angle.

Once we began on-orbit operations we realized that two effects which we had neglected were actually significant.
1) The φ dependence of the effective area at the 5% level, as shown in fig. 2. For long observations this averages out, on shorter times scales it matters if a source was observed preferentially towards the sides or corners of the LAT.
2) Residual signals from out of time cosmic rays which contaminate the event and can cause us to reject good photons. We addressed this by the "*overlay*" technique of adding a sample of periodic triggers to our photon simulations as described in (2). However, this procedure is only accurate on average, orbital variations in particle rates cause variations in A_{eff}. We have found that fraction of time the LAT is occupied with reading out an event and unable to trigger (f_{dead}) is a good tracer of the particle rates and the induced loss of A_{eff}. As shown in fig. 3 we quantify this effect as function of energy and include this livetime dependence as a refinement to the IRFs.

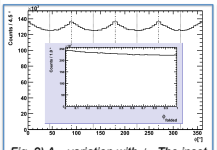

Fig. 2) A_{eff} variation with φ. The inset shows the result of folding φ in the range 0-45° along the dotted and dashed lines in the outer plot.

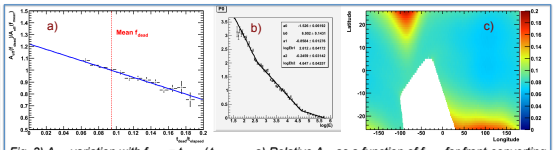

Fig. 3) A_{eff} variation with $f_{dead} = f_{dead} / t_{elapsed}$. a) Relative A_{eff} as a function of f_{dead} for front-converting events at 3.17 GeV. The slope of the line is the percent loss of A_{eff} per percent f_{dead}. b) Evolution of this slope the with energy for front-converting events. c) Map of the mean f_{dead} as a function of orbital position. Note that f_{dead} ranges between 6% and 18%.

2) Event Classes and IRFS sets

Since launch we have used two iterations of the event analysis, Pass 6 and Pass 7 (used for the 2FGL catalog and targeted for public release in July 2011) both of which had photon classes of increasing purity, such as "Transient", "Diffuse" and "Dataclean" for Pass 6.
We have included the improvements described in §1 of this poster to the description of effective area in the P6_V11 set of IRFs, which are in the process of being released at the time of this symposium. Furthermore, the P6_V11 IRF set also includes a scaling correction to the A_{eff} which is described in §4.

Event Selection	IRF Sets	A_{eff} Model Components	Status
Pass 6 TRANSIENT Pass 6 DIFFUSE Pass 6 DATACLEAN	P6_V3_TRANSIENT P6_V3_DIFFUSE P6_V3_DATACLEAN	Overlays	Public
Pass 6 DIFFUSE	P6_V11_DIFFUSE	Overlays φ, f_{dead} dependence (§1) A_{eff} correction (§4)	In Release Process (May 2011)
Pass 7 TRANSIENT Pass 7 SOURCE Pass 7 CLEAN Pass 7 ULTRACLEAN	P7TRANSIENT_V6 P7SOURCE_V6 P7CLEAN_V6 P7ULTRACLEAN_v6	Overlays φ , f_{dead} dependence (§1)	Release Date July 2011

Tab. 1) Events selections and Instrument Response Function (IRF) sets for LAT data analysis. Sets in black are recommended for point source analysis, sets in grey for the analysis of short duration transients or diffuse emission for large parts of the sky.

3) Calibration samples

We have used the large statistics available in our flight data set in conjunction with our knowledge of particular astrophysical sources to develop calibration samples on which we can isolate statistically clean samples of γ-rays by subtracting a background sample from a signal sample and evaluating the excess in the signal region.
Tab. 2 lists the calibrations samples we used and fig. 4 shows the signal and background regions for these samples. It is worth noting that we developed these samples to cover the full LAT energy range with some overlap to allow for consistency checks.

Calibration Sample	Background Subtraction Method
Vela pulsar (2 years) 15° ROI, $\theta_{z,vela} < 90°$	Phase-gated
30 Bright, isolated AGN (2 years) 6° ROI, $\theta_z < 105°$, E > 800MeV	Aperture
Earth limb (200 limb-pointed orbits) E > 8 GeV	Zenith Angle cut

Tab. 2) Data samples and background subtraction techniques used to statistically clean sample of photons to validate the MC based A_{eff} tables.

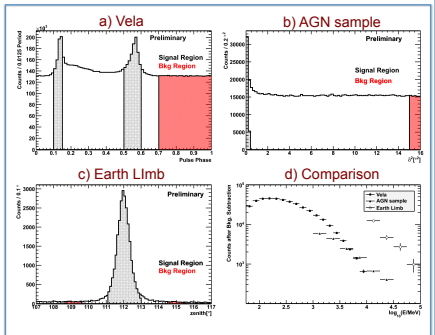

Fig. 4) Calibration Samples. a-c) Vela, AGN and Earth Limb calibration samples for the P7TRANSIENT event selection, including definitions of signal (black) and background (red) regions. d) Signal excess in counts after background subtraction. Note the complementary coverage of the energy range 56MeV – 100 GeV

4) Effective Area Corrections

We measure the efficiency on photons for each cut in our event selection by comparing the signal excess in our calibration samples before and after that cut. We compare that efficiency to the predictions of our Monte Carlo simulations. For every cut in the Pass 6 selections, except one on quality of the event direction reconstruction, the ratio of efficiencies is consistent with unity across the LAT energy range.
We show this exception and resulting corrections to A_{eff} in fig. 5, which we derived using ratios of efficiencies for front and back converting as well as on-axis and off-axis events and interpolating the factors.
As we can see from the inset in fig. 5a for the corresponding cut in Pass 7 (where it was looser) the agreement is much better and does not warrant correcting the A_{eff}.

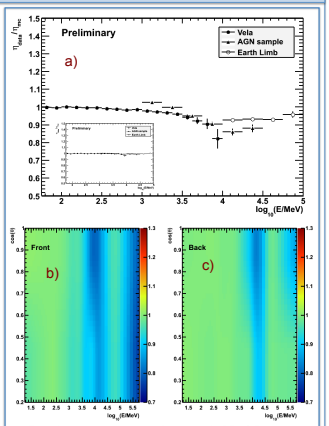

Fig. 5) A_{eff} corrections in P6_V11_DIFFUSE tables. a) Ratio of cut efficiency on flight data to Monte Carlo. The inset shows the same for P7_SOURCE. b,c) A_{eff} Correction factor as a function of angle and energy for both front and back converting events.

5) Consistency Checks

In addition to the evaluation of the event selection cuts, we have performed consistency checks on our event selections.
The largest discrepancies we observe are on fraction of front converting events and the angular (θ) distributions of observed events.
Since these inconsistencies are larger than those for the event selection or coming from sub-system calibrations we take the size of these inconsistencies as the systematic uncertainty on A_{eff}, which is shown in §6.

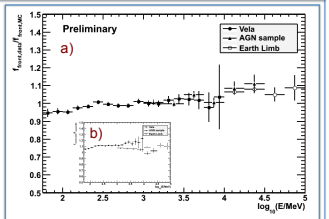

Fig. 6) Consistency checks on P7_SOURCE event selection. a) comparison of fraction of events which convert in the front of the LAT between flight data and MC. b) same comparisons for the fraction of events pointing close to the LAT boresight (cos(θ)>0.7). Note that for the Vela sample we re-weighted simulated events to account for the observing profile in cos(θ).

6) Error Estimates and Caveats

We have used the calibration samples described in §3 to confirm that our description of the A_{eff} of the Fermi-LAT is very accurate when applied over long observation periods. In particular, we validated the MC based predictions of the efficiencies of the various cuts in our events selections. In the one case where we found significant differences we have created corrected versions of the A_{eff} tables. Furthermore, we indentified the small (5-10%) differences between flight data and MC predictions of the fraction of front versus back converting events and the angular distributions of those events as the primary sources of systematic uncertainty in the A_{eff}.

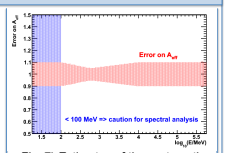

Fig. 7) Estimates of the systematic errors on A_{eff} for P7_SOURCE IRFs.

It is important to point out that for shorter observations all of the effects described in this poster may become significant because of highly non-uniform observing profiles (see fig. 8).

Accordingly we encourage people to familiarize themselves with the improvements to the A_{eff} representations we provided with the P6_V11 and P7 series of IRFs.

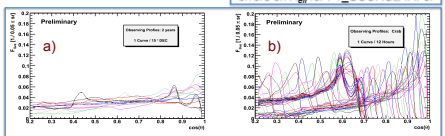

Fig. 8) Example observing profiles as a function of cos(θ). a) Profiles for a variety of declinations for two years of observations. b) Profiles for the crab for a series of 12 hour observations.

References

1. Atwood, W. B. et al., *The Large Area Telescope on the Fermi Gamma-ray Space Telescope Mission*, ApJ, 697, 1071 (2009).
2. R. Rando, *Post-launch performance of the Fermi Large Area Telescope* [arXiv:0907.0626v1]